Eur Radiol (2016) 26:3006–3016
DOI 10.1007/s00330-015-4123-3

ULTRASOUND

Effects of diagnostic ultrasound-targeted microbubble destruction on the homing ability of bone marrow stromal cells to the kidney parenchyma

Gong Wang[1] · Qian Zhang[2] · Zhongxiong Zhuo[1] · Shengzheng Wu[1] · Zheng Liu[1] · Hongmei Xia[1] · Kaibin Tan[1] · Linru Zou[1] · Ling Gan[1] · Yunhua Gao[1]

Received: 22 April 2015 / Revised: 24 August 2015 / Accepted: 16 November 2015 / Published online: 4 December 2015

Abstract

Objectives Bone marrow stromal cells (BMSC) transplantation proves successful in treating kidney disease and injury in many studies. However, their reparative capacity is limited by the poor homing ability in vivo, which is decided mainly by the local expression of chemoattractants. Our study explored the mechanical effects of ultrasound targeted microbubble destruction (UTMD) on BMSCs homing ability in treated kidney tissues.

Methods Rats were injected with red fluorescent protein (RFP)-labelled BMSCs and sonicated with microbubble-mediated ultrasound. Then, we tested kidney micro-environment changes induced and their influence on stem cell homing ability.

Results The results showed that the mechanical effects of UTMD would increase local and transient levels of chemoattractants (i.e. cytokines, integrins and growth factors) in targeted kidney tissues. Transmission electron microscopy showed that vascular endothelial cell was discontinuous in the UTMD group post-treatment, becoming smooth 72 h later. Confocal laser scanning microscopy and RT-PCR showed up to eight times more stem cells in the peritubular regions of experimental kidneys on days 1 and 3 post-treatment compared with the contralateral kidney.

Conclusions These results confirmed that renal micro-environment changes caused by appropriate UTMD may promote BMSC homing ability toward treated kidney tissues without renal toxicity and cell damage.

Key Points

- *This experiment showed a feasible strategy in promoting stem cell homing ability.*
- *The treatment uses diagnostic ultrasound during enhancement with IV microbubbles.*
- *A suitable micro-environment was important for targeted stem cell homing and retention.*
- *The method is effective for stem cell homing to kidney diseases.*
- *More work is required with larger animals before potential human trials.*

Keywords Bone marrow stromal cells · Homing · Ultrasound · Microbubble · Kidney

Gong Wang and Qian Zhang contributed equally to this work.

✉ Yunhua Gao
xqgaoyh@outlook.com

Gong Wang
wanggong127@163.com

Qian Zhang
xqsnzq@163.com

Zhongxiong Zhuo
zzx64120@163.com

Shengzheng Wu
wanggong127@hotmail.com

Zheng Liu
wangg5@uw.edu

Hongmei Xia
550789302@qq.com

Kaibin Tan
546217589@qq.com

Linru Zou
xqgaoyh@gmail.com

Ling Gan
xqgaoyh@hotmail.com

[1] Department of Ultrasound, Xinqiao Hospital, The Third Military Medical University, Chongqing 400037, China

[2] Department of Nephrology, Xinqiao Hospital, The Third Military Medical University, Chongqing, China

Introduction

In recent years, bone marrow derived mesenchymal stem cell (BMSC) therapy has proven to be a promising approach for solving many kidney diseases owing to the paracrine secretion and transdifferentiation ability of these cells [1, 2]. BMSCs were successfully used in animal models of acute renal failure and diabetic nephropathy [3, 4]. Much of the ongoing research utilizes intravenous (IV) injection because it as a non-invasive and promising therapeutic approach to deliver cells to targeted tissues [5]. However, studies show that specific exogenously infused BMSCs home to kidney tissues at very low levels after transplantation (<0.1 % of injected dose), which has limited the effective implementation of BMSC-based strategies [6–8]. Efficacy and targeting of kidney tissue cell engraftment are crucial variables determining BMSC transplantation therapeutic value [9]. Therefore, it is critically important to enhance the abilities of transplanted cells to home to and engraft at targeted renal tissues.

An efficient cell therapy requires transmigration of injected BMSCs across the vascular endothelium; the BMSCs reach the inflamed parenchyma by a process called homing [10, 11]. Similar to that of inflammatory cells, the homing process of BMSCs involves several steps, including chemotactic response by chemokine–chemokine receptor interactions, attachment to vascular endothelial cells and transendothelial migration into the parenchyma [12]. Although the homing mechanisms of BMSCs remain unclear, many studies suggest that regional micro-environmental changes (i.e. the release of chemoattractants and growth factors) associated with inflammation and injury stimulate adhesion of BMSCs and the subsequent transmigration from the vascular into inflamed tissues [13, 14]. Therefore, developing an effective and non-invasive modality to trigger the release of chemoattractants within the local micro-environment is urgently needed to improve the therapeutic applications of BMSCs.

A suitable local micro-environment plays an important role in the migration and survival of transplanted stem cells [15]. Tang et al. showed that a mild inflammatory response caused by microbubble (MB) destruction by 1.0 W/cm^2 ultrasound can increase the homing of BMSCs to acute kidney injury tissue and improve kidney recovery [16]. However, excessive inflammatory infiltration may lead to cell apoptosis and necrosis, which is a disadvantage for BMSC therapy [17]. Compared to the focused ultrasound therapy apparatus used by many researchers, diagnostic ultrasound devices have less output and an appropriate image monitoring system, which is more convenient for mediating targeted MB destruction. We hypothesize that the kidney micro-environment will be altered by UTMD, thereby providing a suitable condition for BMSC delivery in kidney disease therapy.

The purpose of this study was to investigate the possibility of increasing BMSC homing ability through transient elevations of chemoattractants (chemokines, adhesion and trophic factors) by using diagnostic ultrasound coordinated with IV injection of microbubbles.

Materials and methods

Microbubble

Lipid-coated MBs filled with perfluoropropane were prepared at our department as previously described [18]. The mean diameter of the microbubble was 2 μm, and 98 % of the particles had diameters less than 5 μm. The bubbles were diluted with saline to a concentration of 7×10^9/mL before use. Liu et al. showed that it had no significant influence on blood pressure and kidney function [18].

Rat BMSCs culture and labelling

Ninety-eight Sprague–Dawley rats (6–8 weeks old) were provided by the Center for Experimental Animals of Xinqiao Hospital. The experimental protocol conformed to the guidelines for the care and use of laboratory animals (NIH Publication No. 85–23, revised 1996). BMSCs were obtained from the femur and tibia and pooled into one single cell suspension. The cells were then cultured (37 °C, 5 % CO_2) with α-MEM (Hyclone, Logan, UT, USA) medium containing 10 % fetal bovine serum (Gibco, USA). Non-adherent cells were removed after 12 h. Once cells reached 80 % confluency, they were passaged with 0.25 % trypsin–EDTA solution (Gibco, USA) and subcultured. Cells at passage 3 were used for subsequent experiments. Flow cytometry analysis was performed to ensure BMSCs were positive for BMSC surface markers and negative for non-BMSC markers.

To track the transplanted BMSCs in kidney tissues, cells were transfected with lentiviral vectors carrying red fluorescent protein (RFP, Invitrogen Trade Co. Ltd, Shanghai, China) as a cell tracker. Briefly, BMSCs were seeded in 6-well plates at a concentration of 10^5 cells/well. The next day, 1 mL complete medium per well containing viral vectors were added at an MOI (multiplicity of infection) of 10. We observed the infected BMSCs by confocal laser scanning microscopy (CLSM, TCS SP5, Leica, Germany).

Experimental protocols

All experimental rats were fixed in left lateral position after satisfactory anaesthesia with intraperitoneal injection of 2 % pentobarbital sodium (40 mg/kg). Only the right kidney was irradiated, and the left kidney served as internal control. A 9L4 transducer with a frequency of 8 MHz from a clinical Siemens 2000 Dimension ultrasound instrument (Siemens, Germany) was used for two-dimensional echography and Doppler

imaging (Fig. 1a–c). We injected 0.05 mL/kg MBs to evaluate the kidney blood perfusion condition (Fig. 1d, e). Then, we switched to a 4P1 transducer with a frequency of 1.75 MHz and a mechanical index (MI) of 1.4, and placed it vertically above the kidney and irradiated for 5 min (Fig. 1f). Immediately after ultrasound exposure, RFP-labelled BMSCs (1×10^6) were resuspended in 2 mL PBS and injected through the tail vein. The kidney micro-environmental changes induced by UTMD were detected by assessing chemoattractant expression (chemokines, adhesion and trophic factors). The expression of stromal cell derived factor-1 (SDF-1), vascular cell adhesion molecule-1 (VCAM-1), E-selectin and vascular endothelial growth factor (VEGF) proteins were detected by Western blotting.

To assess BMSC homing ability to kidney tissues induced by UTMD, the experimental rats were randomly assigned into four different groups: (i) Con group (n=12; BMSCs injection only); (ii) MB group (n=12; MB was first injected, followed by BMSC injection); (iii) US group (n=12; diagnostic ultrasound sonication followed by BMSC injection) and (iv) UTMD group (n=12; UTMD following by BMSC injection). Four cohorts of rats were killed at 12 h, 24 h, 48 h and 72 h post-treatment. Their kidneys were rapidly dissected. CLSM was used to evaluate the number of BMSCs located in frozen kidney sections (5 mm in thickness). The frozen sections were stained in 5 mg/mL DAPI (4',6-diamidino-2-phenylindole) dihydrochloride (Sigma, USA) for 5 min to mark the nucleus. The survival rates of implanted BMSCs were evaluated in frozen sections by counting six randomly chosen fields under CLSM. The high magnification images from the random fields within each slice were analysed by a commercial computer image analysis system: Image-Pro Plus 5.1 (IPP 5.1 for Windows®; Media Cybernetics, Silver Spring, MD, USA) [19]. In addition, real-time PCR (RT-PCR) analysis was performed to investigate RFP mRNA expression in rat kidney tissues, which could reflect the number of RFP-labelled cells located in kidney tissues.

Real-time PCR

To determine the quantity of RFP-labelled BMSCs deposited in the sonicated kidney tissues, the kidneys were rapidly dissected for RT-PCR analysis. The experimental kidney tissues were weighed, minced and homogenized in a glass homogenizer immediately after kidneys were dissected. DNA was extracted with chloroform and precipitated with ethanol, and the total DNA was assayed by UV absorbance. The oligonucleotide primer sequences were as followings: RFP, 5'-AGTTCCAGTACGGCTCCAAG-3' (sense), and 5'-AGATCTCGCCCTTCAGCAC-3' (anti-sense). We performed RT-PCR assay with target DNA, RFP primer by using a real-time PCR instrument (Applied Biosystems, USA). The left kidney was used for normalization and all items were measured in triplicate.

Western blotting

The expression of SDF-1, VCAM-1, E-selectin and VEGF in kidneys was examined by Western blotting assay. We extracted the proteins using a protein extraction reagent according to the protocol provided by the manufacturer. The proteins were separated by 5 % sodium dodecyl sulfate polyacrylamide gel

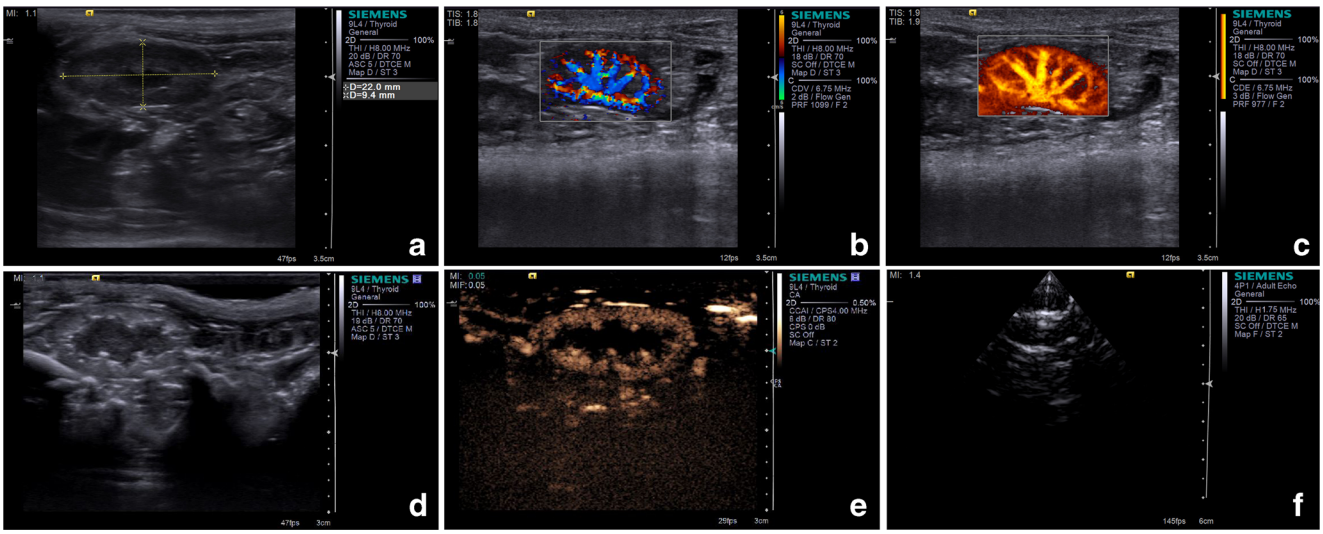

Fig. 1 Ultrasound images of rat kidney targeted for UTMD treatment. We used an 9 L4 transducer with an 8-MHz frequency for two-dimensional ultrasound images (**a**); colour (**b**) and Doppler (**c**) ultrasound images indicate good blood perfusion in targeted kidney tissues. Then, intravenous injected microbubbles arrived in kidney tissues as shown by ultrasound image at 8 MHz (**d**) and contrast-enhanced ultrasound mode (**e**). A 4P1 transducer with a frequency of 1.75 MHz and a mechanical index of 1.4 was switched to continuously irradiate targeted kidney tissues (**f**)

electrophoresis and then transferred to poly(vinylidene fluoride) (PVDF) membranes. Membranes were blocked with 50 mL/L of skim milk in Tris-buffered saline and Tween 20 at room temperature, then incubated with rabbit anti-rat SDF-1 IgG (Abcam, Cambridge, UK), VCAM-1 IgG (Abcam, Cambridge, UK), E-selectin IgG (Abcam, Cambridge, UK) and VEGF IgG (Abcam, Cambridge, UK) at a final dilution of 1:100. The protein bands were normalized with GAPDH. A BioSpectrum Imaging System (Chemi-Smart 3000, France) was used to analyse the optical density of the protein bands.

ELISA analysis

To examine the effects of UTMD in treated kidneys and its ability to increase the levels of cytokines, we divided the rats into two groups (control group and UTMD group; n=12 for each group). The rats were killed at 12 h, 24 h, 48 h and 72 h post-UTMD treatment for cytokine analysis. The amounts of interleukin (IL)-1 alpha (1α), IL-2, IL-3, IL-4, interferon-γ (IFN-γ), tumour necrosis factor alpha (TNF-α), monocyte chemotactic protein-1 (MCP-1) and macrophage inflammatory protein-1α (MIP-α) were measured using an enzyme-linked immunosorbent assay (ELISA, R&D Systems, Minneapolis, MN, USA)-based method according to the manufacturer's instructions. All measurements were performed in triplicate.

Transmission electron microscopy

To assess the possible mechanisms for kidney microenvironment changes, we investigated ultra-morphology changes of kidney vascular endothelial cells using transmission electron microscopy (TEM). Rat kidneys were removed at 0, 12, 24, 48 and 72 h after UTMD treatment (n=3 for each group). We cut the renal cortices into 1-mm pieces and fixed them in 2 % glutaraldehyde (Beyotime, Shanghai, China). The samples were then post fixed, dehydrated and embedded in epoxy resin. The ultra-thin sections (50 nm) were double-stained with uranyl acetate and lead citrate, then examined with a transmission electron microscope (Hitachi Inc., Tokyo, Japan) by a pathologist who was blinded to our study.

Histopathology

The kidney tissues of rats in the study were obtained before UTMD treatment and at 0, 12, 48 and 72 h after UTMD treatment (n=3 for each group). The tissues were fixed in 10 % neutral buffered formalin and embedded in paraffin. Then, 5-μm-thick sections were stained with haematoxylin and eosin (H&E) and periodic acid–Schiff (PAS) for histopathologic examination. The sections were examined under a light microscope (×400) by a pathologist who was blinded to our study.

Renal function analysis

To evaluate renal function changes under UTMD treatment, rat blood was drawn from the tail vein at 12, 24, 48 and 72 h post-UTMD treatment (n=3 for each group). The levels of blood urea nitrogen (BUN) and serum creatinine (Scr) were measured in the Xinqiao Hospital clinical laboratory using an automatic biochemical analyzer (Hitachi, Japan).

Statistical analysis

All data (mean±standard deviation) was analysed to identify statistical significant differences between multiple groups using one-way analysis of variance (ANOVA). An alpha value of P<0.01 was considered statistically significant. The statistical analysis was performed using SPSS 13.0 software (SPSS Inc., Chicago, IL, USA).

Results

Culture, identification and labelling of rat BMSCs

Most of the primary cultured rat BMSCs were spindle shaped and became more homogeneous in shape after two passages (Fig. 2a, b). BMSCs transfected with lentiviral vectors carrying RFP showed bright red fluorescence under CLSM (Fig. 2d, e). Flow cytometry (FCM) showed that the level of RFP expression in BMSCs was approximately 97±0.53 % (Fig. 2f, g). These expanded BMSCs were positive for BMSC surface antigens CD29 (98.9 %, Fig. 2h), CD44 (96.8 %, Fig. 2i) and CD90 (95.9 %, Fig. 2j), and negative for the leukocyte common antigens CD34 (1.09 %, Fig. 2k) and CD45 (1.20 %, Fig. 2l).

Assessment of BMSCs engrafted to kidney

CLSM images showed that RFP-labelled BMSCs were mostly localized in the extravascular region of the interstitial capillary bed. Only a small number of deposited BMSCs were observed in glomeruli (Fig. 3a). Quantification analysis of RFP-labelled BMSCs in renal tissue showed that the number of engrafted RFP-labelled BMSCs in the UTMD group (91.5 ±3.8 cells) was statistically greater than in the US group (19.3 ±1.6 cells), MB group (19.8±2.12 cells) and Con group (19.0 ±1.64 cells) 12 h post-treatment (P<0.01). No significant difference was found between the US group, MB group and Con group. The number of engrafted BMSCs in kidney tissues was greater in the UTMD group than other groups at 24, 48 and 72 h post-treatment (Fig. 3b).

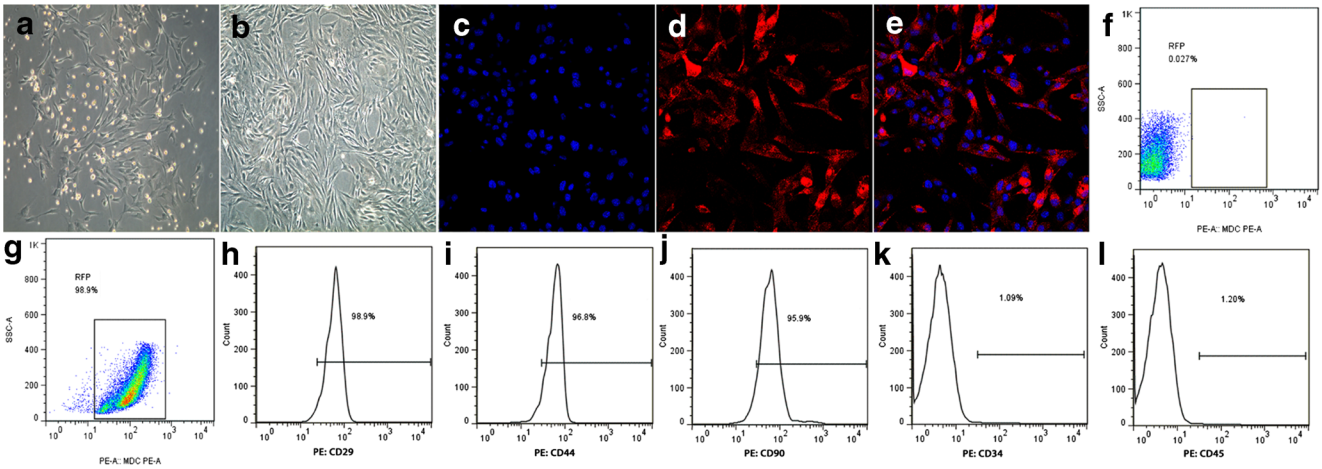

Fig. 2 BMSCs culture and characteristics. After 10–14 days of primary culture (**a**), the subcultured BMSCs at passage 3 became more homogeneous and spindle shaped and proliferated to approximately 80 % confluence (×100) (**b**). Bmscs were transfected with lentiviral vectors carrying RFP as a cell tracker. CLSM images showed red fluorescence representing RFP expression in experimental BMSCs, and blue fluorescence showed nuclear staining (**c**–**e**). FCM analysis showed RFP expression efficiency (the number of cells expressing RFP/number of cells in total) in experimental BMSCs 48 h after transfection was 98.9 % (**g**) compared to non-RFP-transfected control cells (**f**). The phenotype of BMSCs was shown to be positive for CD29 (98.9 %, **h**), CD44 (96.8 %, **i**) and CD90 (95.9 %, **j**) and negative for CD34 (1.09 %, **k**), CD45 (1.20 %, **l**)

The expression of RFP mRNA in each group showed the same trend as with CLSM images. The results revealed that RFP mRNA expression was increased in the UTMD group at 12, 24, 48 and 72 h post-treatment compared with the US group, MB group and Con group ($P<0.01$). No significant difference was found between the US group, MB group and Con group (Fig. 3c).

Kidney micro-environmental changes induced by UTMD

Western blotting results indicated that UTMD treatment markedly increased and E-selectin, VCAM-1, SDF-1 and VEGF levels at 12, 24 and 48 h post-treatment compared to the control group ($P<0.01$). They returned to normal levels by 72 h post-treatment ($P>0.05$) (Fig. 4). This indicated that renal micro-environments could be altered transiently and be recoverable through UTMD treatment.

Cytokines

ELISA-based cytokine array (Fig. 5a) showed that certain cytokine expression was increased at 12, 24 and 48 h post-UTMD treatment compared to the control

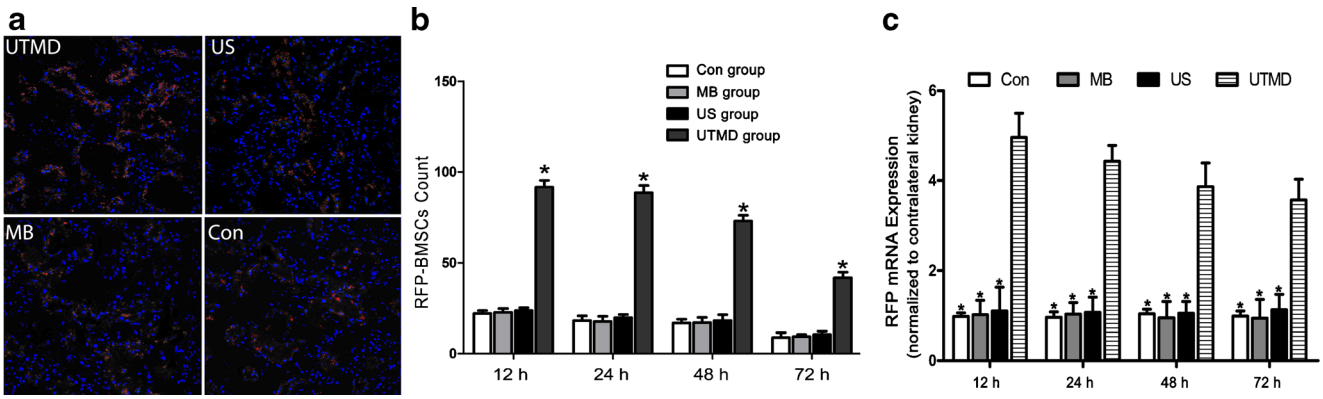

Fig. 3 Transplanted RFP-labelled BMSCs dwelling in UTMD-treated kidneys. **a** Four CLSM images depicting engrafted BMSCs in sonicated kidney tissues for four different experimental groups as mentioned at 12 h post-treatment. Red fluorescence represents RFP and blue fluorescence represents the cell nucleus. These images show that the deposition of RFP in kidney tissues was most clearly observable in the UTMD group and was mostly located in the extravascular region of interstitial capillary. **b** Quantitative analysis by Image-Pro Plus 5.1 revealed that the number of RFP-labelled BMSCs in the UTMD group was significantly more than in other groups at 12, 24, 48 and 72 h post-treatment. The *asterisk* indicates a significant difference compared to the Con group; *$P<0.01$. **c** RT-PCR analysis revealed that the quantity of RFP mRNA expression in the UTMD group was significantly more than in the other groups at 12, 24, 48 and 72 h post-treatment. No significant difference was found between the Con group, MB group and US group. The *asterisk* indicates a significant difference compared to the UTMD group; *$P<0.01$

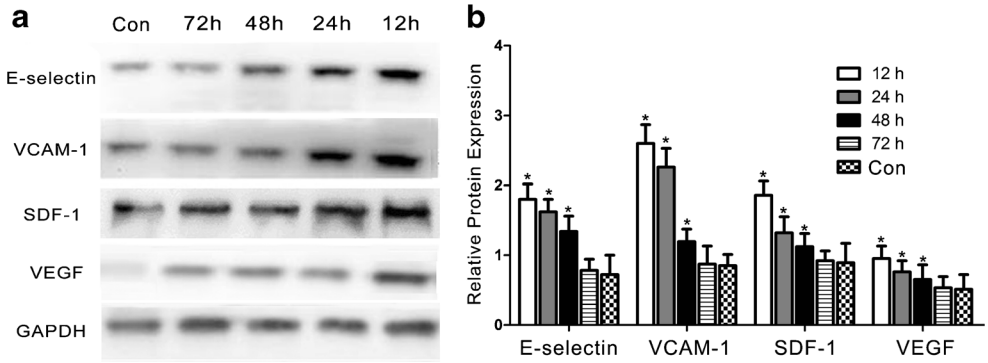

Fig. 4 Western blot analysis of protein expression in UTMD-treated kidneys. **a** The representative Western blots for the expression of E-selectin, VCAM-1, SDF-1 and VEGF in the kidneys before and after UTMD treatment, which were normalized to GAPDH. **b** The expression of E-selectin, VCAM-1, SDF-1 and VEGF at 12, 24, and 48 h post-treatment was significantly higher than at 0 h and returned to normal levels by 72 h post-treatment. The *asterisk* indicates a significant difference compared with the Con group (0 h): *$P<0.01$

group; these cytokines included IL-1α, IL-2, IL-3, IFN-γ, TNF-α, MCP-1 and MIP-α. The levels of cytokine expression in UTMD-treated kidneys returned to control kidney levels by 72 h post-treatment ($P>0.05$; Table 1).

Transmission electron microscopy

Ultra-structural changes observed by TEM indicated that part of the renal interstitial vascular endothelial cell membranes became discontinuous, deficient and roughened at 12, 24 and 48 h post-UTMD treatment compared to the control group (Fig. 6a, c–e). The integrity of the renal capillary wall gradually recovered over time. Thus, 72 h after UTMD treatment, the vascular endothelial cell membranes had become smooth and intact again (Fig. 6b). The findings suggested that the mild vascular endothelial cell injury may be responsible for renal micro-environment changes caused by UTMD treatment.

Histopathology and renal function analysis

There were no significant differences in the serum BUN and Scr levels at 12, 24, 48 and 72 h post-UTMD treatment compared to their respective pretreatment values ($P>0.05$; Fig. 5b; Table 1). HE staining showed no signs of cytolysis or cell necrosis following UTMD treatment; only mild haemorrhage and inflammation were observed after UTMD treatment (Fig. 7a). PAS staining demonstrated no obvious signs of renal tissue disorganization after UTMD treatment (Fig. 7b).

Discussion

Although many studies have shown the curative effect of BMSC therapy, their clinical application was restricted by insufficient numbers of engrafted cells remaining in targeted renal tissues [20, 21]. Cheng et al. found that the IV injected BMSCs were largely localized in pulmonary capillaries, and only a small number of cells could home into renal tissues and

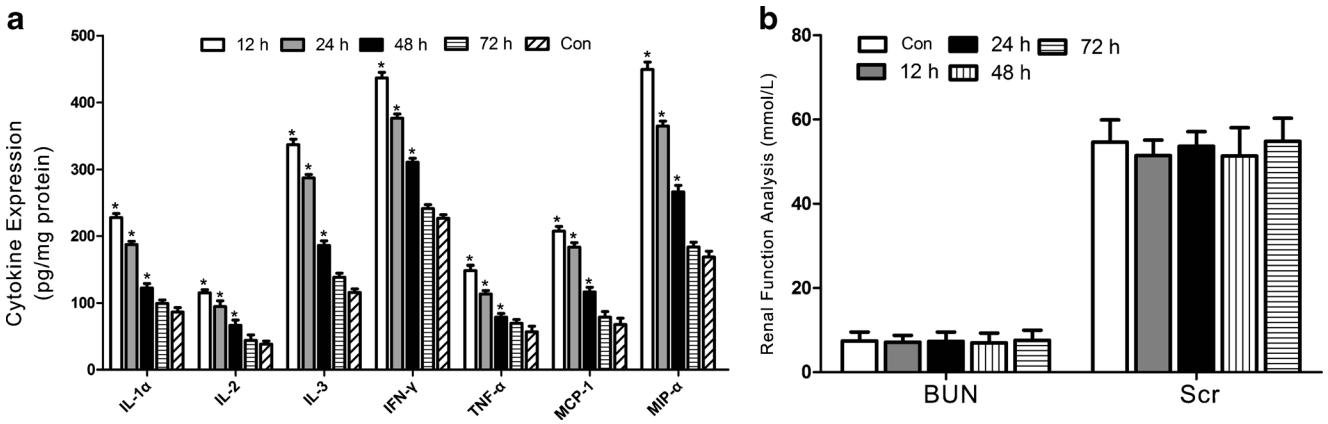

Fig. 5 Cytokine expression and renal function analysis in UTMD-treated kidneys. **a** The expression of IL-1α, IL-2, IL-3, IFN-γ, TNF-α, MCP-1 and MIP-α at 12, 24 and 48 h post-UTMD treatment was significantly higher than in the Con group ($P<0.01$) and returned to normal levels by 72 h post-treatment ($P>0.05$). The *asterisk* indicates a significant difference compared with Con group (0 h): *$P<0.01$. **b** There was no significant difference in the BUN and Scr levels at 12, 24, 48 and 72 h post-UTMD-treatment compared to the Con group

Table 1 Quantitatively analysis of cytokines and renal function at 12 h, 24 h, 48 h and 72 h post-UTMD treatment

Cytokine analysis															
Cytokines	Con			12 h			24 h			48 h			72 h		
	Mean	SD	N	Mean	SD	N	Mean	SD	N	Mean	SD	N	Mean	SD	N
IL-1α	86.3	6.8	3	227.6	6.2	3	187.4	4.8	3	112.6	6.6	3	99.4	5.2	3
IL-2	38.4	4.6	3	115.4	4.6	3	94.5	8.7	3	66.5	7.9	3	43.8	8.4	3
IL-3	115.9	5.3	3	336.7	8.4	3	287.3	5.3	3	186	6.8	3	138.6	6.1	3
IFN-γ	226.8	5.4	3	436.8	8.6	3	376.4	6.4	3	310.5	5.9	3	241.4	5.8	3
TNF-α	56.8	8.4	3	148.6	7.8	3	113.5	5.2	3	78.7	5.6	3	69.4	5.8	3
MCP-1	67.8	9.4	3	207.6	6.7	3	183.4	6.7	3	116.5	6.9	3	78.6	8.6	3
MIP-α	168.6	8.6	3	449.8	10.8	3	364.8	7.4	3	266.4	9.8	3	183.6	7.3	3
Renal function analysis															
	Con			12 h			24 h			48 h			72 h		
	Mean	SD	N	Mean	SD	N	Mean	SD	N	Mean	SD	N	Mean	SD	N
BUN	7.4	2.1	3	7.1	1.6	3	7.4	2.2	3	6.94	2.3	3	7.56	2.4	3
Scr	54.6	5.3	3	51.4	3.7	3	56.7	3.5	3	51.3	6.7	3	54.8	5.5	3

exhibit transient survival [22]. Many methods have been developed to enhance stem cell homing ability. Image-guided implantation of stem cells into targeted tissues was previously used because the injected BMSCs could bypass the initial pulmonary trapping. However, more than 90 % of cell death will occur as a result of lack of nutrition and oxygen [23]. Intra-arterial injections could also bypass the initial pulmonary trapping to areas of interest with homing efficiency dependent on blood perfusion. However, this therapy modality may increase the potential of micro-infarcts and ischaemia induced by passive trapping of stem cells [24]. IV injection showed lower homing efficiency but with minimal injury [25, 26]. Therefore, it is valuable to develop an effective and safe method to enhance BMSC homing ability for successful stem cell therapies.

Rapid progress has been made in evaluating BMSC therapeutic potency in clinical trials and experimental animal disease models. However, understanding the mechanisms involved in stem cell bio-distribution and homing in vivo has been slow to develop [8]. BMSCs may localize to inflamed tissue by active homing mechanisms, which are thought to be analogous to leukocyte homing to specific inflamed tissues [27, 28]. Active homing may involve the rolling and tethering of BMSCs to integrins highly expressed in endothelial cells, followed by migration into the parenchyma as a result of locally expressed cytokines gradients in pathology [29].

UTMD is reportedly a novel non-invasive therapy modality for the delivery of drugs or genes in vivo [30, 31]. The mechanism may be concerned with the widened capillary endothelium gap, the ruptured capillary and the increased vascular permeability [32]. The inflammatory response caused by repair of these injuries would release some types of cytokines from subsequent inflammatory cells, and this may play a vital role in the homing and survival of BMSCs [33, 34]. A mild inflammatory response may be helpful for the homing and mobilization of BMSCs, while an excessive inflammatory response will induce cell necrosis and haemorrhage [15, 16]. We selected diagnostic ultrasound, which has real-time imaging capability and less output compared to therapeutic ultrasound, to induce local UTMD in kidney tissues.

In this study, we investigated the micro-environment changes and homing of ability of BMSCs induced by UTMD in irradiated kidneys. The number of RFP-labelled BMSCs in the UTMD group was much larger than those of Con, MB and US groups at 12, 24, 48 and 72 h post-treatment. Histological examination demonstrated that neither kidney architecture changes nor any cell apoptosis induced in the targeted kidney was found; only a mild, transient inflammatory response occurred, which was recoverable after UTMD treatment. Renal function analysis indicated no significant difference in the post-treatment serum BUN and Scr levels compared with pre-treatment values. These findings suggested that diagnostic UTMD was effective for homing of BMSCs to kidney parenchyma without obvious tissue damage. This is largely because the diagnostic ultrasound apparatus was of lower power (the maximum acoustic intensity, $I_{SPTA} \leq 539$ mW/cm^2) compared to therapeutic ultrasound (intensity between 0.2 and 3 W/cm^2) [35]. To apply this therapeutic modality for human kidney disease treatment, additional obstacles must be overcome. Firstly, a new diagnostic ultrasound transducer should be well designed so that the acoustic beam could achieve optimal treatment for human beings. Secondly, we should optimize the parameters involved to get the maximum treatment. The sonication duration, injected MB dose and mechanical index (MI) of the ultrasound device might affect the therapeutic effect of UTMD. Thirdly, the attenuation of acoustic intensity will be higher in bigger animals compared to rats, so we should study suitable parameters for future application of this

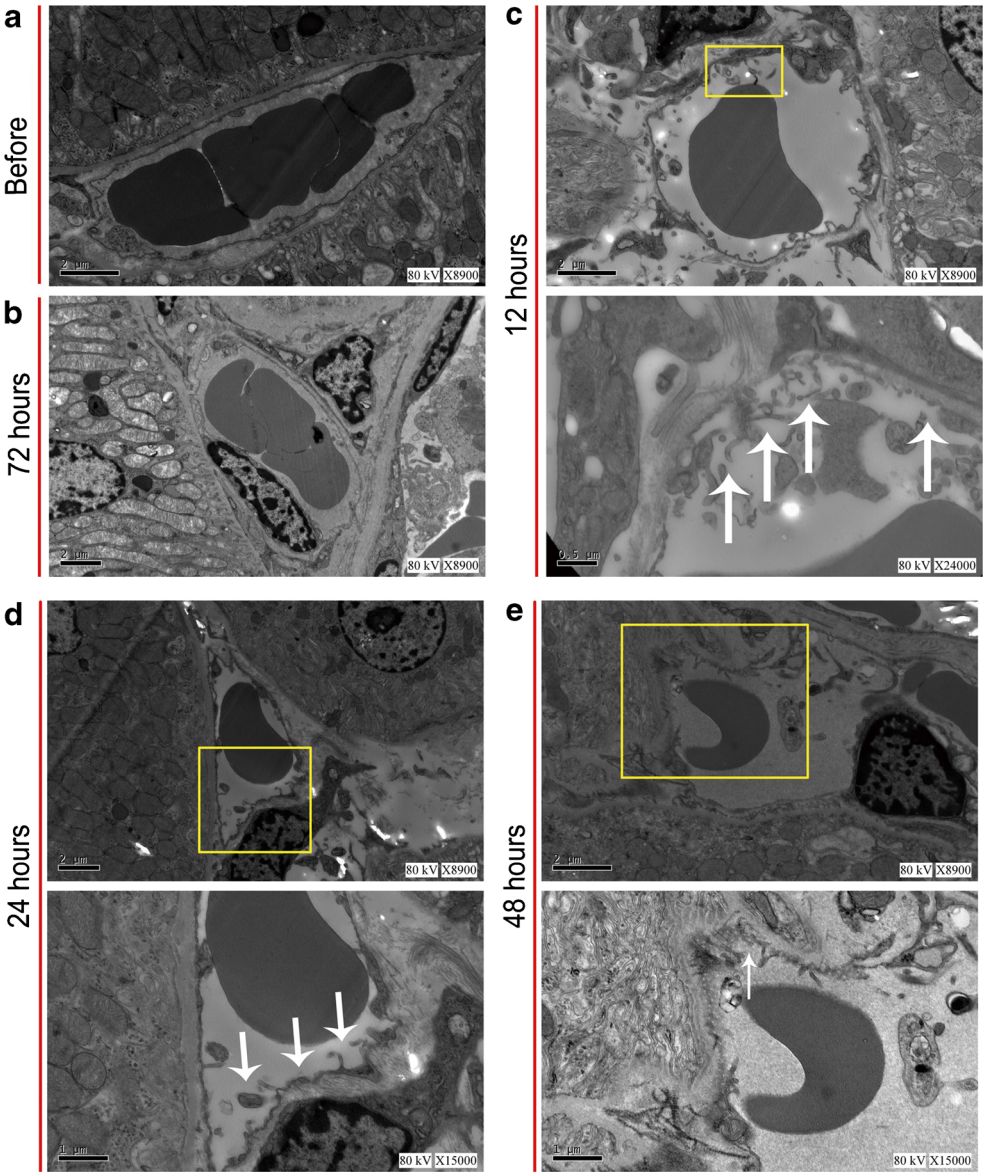

Fig. 6 Assessment of renal vascular endothelium changes under microbubble-mediated ultrasound irradiation by TEM. **a** The endothelial cells of renal interstitial capillary showed an intact and smooth surface before UTMD treatment. **b** The integrity of renal capillary walls recovered from UTMD and became smooth and intact again 72 h after UTMD treatment. **c**–**e** Part of the renal interstitial capillary endothelium is damaged by UTMD. The vascular walls have become thinner, discontinuous, deficient and roughened at 12, 24 and 48 h post-UTMD-treatment, respectively

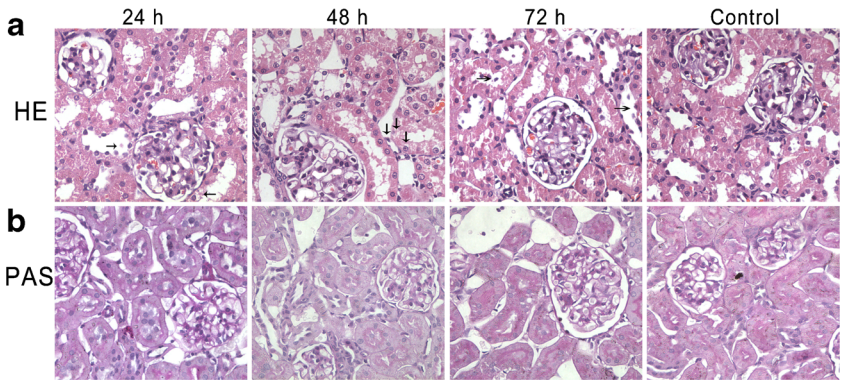

Fig. 7 HE and PAS staining showed changes in UTMD-treated kidney tissues. **a** HE staining showed no signs of haemorrhage, cytolysis or cell necrosis in the Con group and UTMD-treated kidney tissues (magnification ×400). Only mild inflammatory responses were found; these were transient and recoverable after UTMD treatment. The *black arrows* indicate inflammatory cells around kidney capillary tissues. **b** PAS staining showed no relevant signs of renal tissue disorganization between the Con group or UTMD treated kidney tissues (magnification ×400)

technology for potential application in human beings. Fourthly, in-depth safety studies should be performed in the future. Last, further study is needed to clarify the precise morphology and molecular biological profile of UTMD-treated kidney. Tebebi et al. have investigated the characteristic molecular responses to mechanical pulsed focused ultrasound (pFUS) for establishing local gradients of cytokines and chemokines in treated skeletal muscle that subsequently allow infused BMSCs to migrate into the parenchyma. The results showed that TNF-α drives cyclooxygenase-2 (COX2) signalling, which is induced through mechanotransduction, may be responsible for the established local cytokine gradients [36]. Further study is needed to explore whether COX2 and the NFkB pathway are the possible mechanisms for UTMD causing release of chemoattractants in the kidney in our study.

Our study showed that diagnostic UTMD may transiently increase the expression of some inflammatory cytokines, endogenous angiogenic growth factors and adhesion molecules. We selected four representative cytokines (VEGF, SDF-1, VCAM-1 and E-selectin) as the major diagnostic factors and tried to elucidate the local kidney micro-environment changes [37–40]. These cytokines were transiently increased at 12, 24 and 48 h post-treatment compared to the control group and returned to normal levels by 72 h. Some cytokines, including IL-1α, IL-2, IL-3, IL-4, IFN-γ, TNF-α, MCP-1 and MIP-α, showed similar changing trends in an ELISA-based cytokine array [41]. The ruptured capillary observed by TEM and subsequent inflammatory response might induce different types of cytokines that may change the local kidney micro-environment. We hypothesize that the potential mechanism has something to do with this fact, which played a vital role in the homing and survival of BMSCs in kidney tissues.

Active targeting of IV injected BMSCs to targeted tissues has been accompanied successfully by local radiation therapy and pFUS. Low-dose radiation to tumours has been recommended to increase the tropism of BMSCs for tumour satellite micro-metastases [42, 43]. However, radiation may result in unwanted damage of surrounding tissues as it cannot focus on deep tissues. Ziadloo et al. showed that pFUS (spatial average, temporal peak intensity=2667 W/cm^2; duty cycle=5 %) could improve BMSC therapies for targeted kidney tissues by establishing local chemoattractant gradients [44]. Burks et al. showed that repeated application of pFUS could increase the magnitude of homing of stem cells in skeletal muscle [45]. Our results regarding the chemoattractant response showed the same trend compared as those of Ziadloo and Burks. However, FUS units are currently only approved by the US Food and Drug Administration for possible application in limited areas, like uterine fibroid and the early phase of malignancy [46, 47]. Further study is needed before the potential clinical application of enhancing BMSCs engraftment by pFUS in human beings, particularly in relation to understanding their unclear biological effects and side effects in vivo. Diagnostic UTMD may be more readily available in many countries compared with other methods, because most departments have access to diagnostic ultrasound devices than to pFUS and image-guided focused ultrasound etc.

An ideal stem cell homing strategy capitalizes on enhancement of chemoattractants in targeted tissues without obvious injury. In this study, we demonstrated that diagnostic ultrasound-mediated UTMD could increase the engraftment of IV injected BMSCs by releasing some cytokines within 48 h without any side effect in targeted kidney tissues. These findings could be explained by the enhanced acoustic cavitation resulting from the reversible and non-destructive interactions between UTMD and biological tissue. We hypothesize that the ruptured capillary walls and the increased cytokine expression can promote the attachment of stem cells onto the injured endothelium, and some of the increased cytokine gradient may be helpful for stem cell migration. While this study was performed in normal kidney tissues, attempting to direct BMSC migration during pathology may be complicated by endogenous inflammation associated with increased inflammatory cells and cytokines. Therefore, we should continue to explore whether UTMD can induce enhanced stem cell homing ability and similar molecular changes in kidney diseases.

Acknowledgments The scientific guarantor of this publication is Professor Yunhua Gao. The authors of this manuscript declare no relationships with any companies whose products or services may be related to the subject matter of the article. This study has received funding from the Natural Science Foundation of China (No: 81501485). One of the authors has significant statistical expertise. Institutional review board approval was obtained. Approval from the institutional animal care committee was obtained. Methodology: prospective, randomised controlled trial/experimental, performed at one institution.

References

1. Liu N, Tian J, Cheng J, Zhang J (2013) Effect of erythropoietin on the migration of bone marrow-derived mesenchymal stem cells to the acute kidney injury microenvironment. Exp Cell Res 13:2019–2027
2. Li D, Wang N, Zhang L, Hanyu Z, Xueyuan B, Fu B, Shaoyuan C, Zhang W, Xuefeng S, Li R (2013) Mesenchymal stem cells protect podocytes from apoptosis induced by high glucose via secrection of epithelial growth factor. Stem Cell Res Ther 4:2–11
3. Fang Y, Tian X, Bai S, Fan J, Hou W, Tong H, Li D (2012) Autologous transplantation of adipose-derived mesenchymal stem cells ameliorates streptozotocin-induced diabetic nephropathy in rats by inhibiting oxidative stress, pro-inflammatory cytokines and the p38 MAPK signaling pathway. Int J Mol Med 30:85–92
4. Park JH, Hwang I, Hwang SH, Han H, Ha H (2012) Human umbilical cord blood-derived mesenchymal stem cells prevent diabetic renal injury through paracrine. Diabetes Res Clin Pract 98:465–473
5. Harting MT, Jimenez F, Xue H, Fischer UM, Baumgartner J, Dash PK, Cox CS (2009) IV mesenchymal stem cell therapy for traumatic brain injury. J Neurosurg 110:1189–1197

6. Lee RH, Pulin AA, Seo MJ, Kota DJ, Ylostalo J, Larson BL, Semprun-Prieto L, Delafontaine P, Prockop DJ (2009) IV hMSCs improve myocardial infarction in mice because cells embolized in lung are activated to secrete the anti-inflammatory protein TSG-6. Cell Stem Cell 5:54–63
7. Duffield JS, Park KM, Hsiao LL, Kelley VR, Scadden DT, Ichimura T, Bonventre JV (2005) Restoration of tubular epithelial cells during repair of the postischemic kidney occurs independently of bone marrow-derived stem cells. J Clin Invest 115:1743–1755
8. Deak E, Seifried E, Henschler R (2010) Homing pathways of mesenchymal stromal cells (MSCs) and their role in clinical applications. Int Rev Immunol 29:514–529
9. Lotfinejad P, Shamsasenjan K, Movassaghpour A, Majidi J, Baradaran B (2014) Immunomodulatory nature and site specific affinity of mesenchymal stem cells: a hope in cell therapy. Adv Pharm Bull 4:5–13
10. Zhao W, Phinney DG, Bonnet D, Dominici M, Krampera M (2014) Mesenchymal stem cell biodistribution, migration, and homing in vivo. Stem Cells Int 29:292–294
11. Stefan B, Hans D, Monika L, Ulrich G, Johanna G, Bruno H, Markus V, Dirk A, Martina S, Reinhard K, Christian R, Robert D (2013) Enhanced stem cell migration mediated by VCAM-1/VLA-4 interaction improves cardiac function in virus-induced dilated cardiomyopathy. Basic Res Cardiol 108:388–402
12. Chavakis E, Urbich C, Dimmeler S (2008) Homing and engraftment of progenitor cells: a prerequisite for cell therapy. J Mol Cell Cardiol 45:514–522
13. Karp JM, Leng Teo GS (2009) Mesenchymal stem cell homing: the devil is in the details. Cell Stem Cell 4:206–216
14. Hills CE, Squires PE (2011) The role of TGF-β and epithelial-to mesenchymal transition in diabetic nephropathy. Cytokine Growth Factor Rev 22:131–139
15. Greco SJ, Rameshwar P (2008) Microenvironmental considerations in the application of human mesenchymal stem cells in regenerative therapies. Biologics 2:699–705
16. Tang H, Wang Z, Li Q, Ran H, Zheng Y, Ren J, Ling Z, Li A, Zhao B (2012) Targeted delivery of bone mesenchymal stem cells by ultrasound destruction of microbubble promotes kidney recovery in acute kidney injury. Ultrasound Med Biol 4:661–669
17. Hu X, Wang J, Chen J, Luo R, He A, Xie X, Li J (2007) Optimal temporal delivery of bone marrow mesenchymal stem cells in rats with myocardial infarction. Eur J Cardiothorac Surg 31:438–443
18. Liu P, Wang X, Zhou S, Hua X, Liu Z, Gao Y (2011) Effects of a novel ultrasound contrast agent with long persistence on right ventricular pressure: comparison with SonoVue. Ultrasonics 14:210–214
19. Salinas-Navarro M, Jiménez-López M, Valiente-Soriano FJ, Alarcón-Martínez L, Avilés-Trigueros M, Mayor S, Holmes T, Lund RD, Villegas-Pérez MP, Vidal-Sanz M (2009) Retinal ganglion cell population in adult albino and pigmented mice: a computerized analysis of the entire population and its spatial distribution. Vis Res 49:637–647
20. Detante O, Moisan A, Dimastromatteo J, Richard MJ, Riou L, Grillon E, Barbier E, Desruet MD, De Fraipont F, Segebarth C, Jaillard A, Hommel M, Ghezzi C, Remy C (2009) IV administration of 99mTc-HMPAO-labeled human mesenchymal stem cells after stroke: in vivo imaging and biodistribution. Cell Transplant 18: 1369–1379
21. Ankrum J, Karp JM (2010) Mesenchymal stem cell therapy: two steps forward, one step back. Trends Mol Med 16:203–209
22. Cheng K, Rai P, Plagov A, Lan X, Kumar D, Salhan D, Rehman S, Malhotra A, Bhargava K, Palestro CJ, Gupta S, Singhal PC (2013) Transplantation of bone marrow-derived MSCs improves cisplatinum-induced renal injury through paracrine mechanisms. Exp Mol Pathol 94:466–473
23. Pawelczyk E, Jordan EK, Balakumaran A, Chaudhry A, Gormley N, Smith M, Lewis BK, Childs R, Robey PG, Frank JA (2009) In vivo transfer of intracellular labels from locally implanted bone marrow stromal cells to resident tissue macrophages. PLoS One 4: 671–682
24. Walczak P, Zhang J, Gilad AA, Kedziorek DA, Ruiz-Cabello J, Young RG, Pittenger MF, van Zijl PC, Huang J, Bulte JW (2008) Dual-modality monitoring of targeted intraarterial delivery of mesenchymal stem cells after transient ischemia. Stroke 39:1569–1574
25. Bos C, Delmas Y, Desmoulière A, Solanilla A, Hauger O, Grosset C, Dubus I, Ivanovic Z, Rosenbaum J, Charbord P, Combe C, Bulte JW, Moonen CT, Ripoche J, Grenier N (2004) In vivo MR imaging of intravascularly injected magnetically labeled mesenchymal stem cells in rat kidney and liver. Radiology 233:781–789
26. Schrepfer S, Deuse T, Reichenspurner H, Fischbein MP, Robbins RC, Pelletier MP (2007) Stem cell transplantation: the lung barrier. Transplant Proc 39:573–576
27. Sohni A, Verfaillie CM (2013) Mesenchymal stem cells migration homing and tracking. Stem Cells Int 10:130–138
28. Kavanagh DPJ, Robinson J, Kalia N (2014) Mesenchymal stem cell priming: fine-tuning adhesion and function. Stem Cell Rev Rep 10: 14–27
29. Steingen C, Brenig F, Baumgartner L, Schmidt J, Schmidt A, Bloch W (2008) Characterization of key mechanisms in transmigration and invasion of mesenchymal stem cells. J Mol Cell Cardiol 44: 1072–1084
30. Zhou S, Li S, Liu Z, Tang Y, Wang Z, Gong J, Liu C (2010) Ultrasound-targeted microbubble destruction mediated herpes simplex virus-thymidine kinase gene treats hepatoma in mice. J Exp Clin Cancer Res 29:170–176
31. Li P, Zheng Y, Ran H, Tan J, Lin Y, Zhang Q, Ren J, Wang Z (2012) Ultrasound triggered drug release from 10-hydroxycamptothecin-loaded phospholipid microbubbles for targeted tumor therapy in mice. J Control Release 162:349–354
32. Liang HD, Tang J, Halliwell M (2010) Sonoporation, drug delivery, and gene therapy. Proc Inst Mech Eng 224:343–361
33. Yoshida J, Ohmori K, Takeuchi H, Shinomiya K, Namba T, Kondo I, Kiyomoto H, Kohno M (2005) Treatment of ischemic limbs based on local recruitment of vascular endothelial growth factor-producing inflammatory cells with ultrasonic microbubble destruction. J Am Coll Cardiol 46:899–905
34. Ghanem A, Steingen C, Brenig F, Funcke F, Bai ZY, Hall C, Chin CT, Nichenig G, Bloch W, Tiemann K (2009) Focused ultrasound-induced stimulation of microbubbles augments site-targeted engraftment of mesenchymal stem cells after acute myocardial infarction. J Mol Cell Cardiol 47:411–418
35. Jackson JK, Pirmoradi FN, Wan CP, Siu T, Chiao M, Burt HM (2011) Increased accumulation of paclitaxel and doxorubicin in proliferating capillary cells and prostate cancer cells following ultrasound exposure. Ultrasonics 51:932–939
36. Tebebi PA, Burks SR, Kim SJ, Williams RA, Nguyen BA, Venkatesh P, Frenkel V, Frank JA (2015) Cyclooxygenase-2 or tumor necrosis factor inhibitor attenuate the mechanotransductive effects of pulsed focused ultrasound to suppress mesenchymal stromal cells homing to healthy and dystrophic muscle. Stem Cells 33: 1173–1186
37. Ponte AL, Marais E, Gallay N, Langonné A, Delorme B, Hérault O, Charbord P, Domenech J (2007) The in vivo migration capacity of human bone marrow mesenchymal stem cells: comparison of chemokine and growth factor chemotactic activities. Stem Cells 25: 737–745
38. Levoye A, Balabanian K, Baleux F, Bachelerie F, Lagane B (2009) CXCR7 heterodimerizes with CXCR4 and regulates CXCL12-mediated G protein signaling. Blood 113:6085–6093
39. Thankamony SP, Sackstein R (2011) Enforced hematopoietic cell E- and L-selectin ligand (HCELL) expression primes

transendothelial migration of human mesenchymal stem cells. Proc Natl Acad Sci 108:2258–2263
40. Krause DS, Lazarides K, Lewis JB, von Andrian UH, van Etten RA (2014) Selectins and their ligands are required for homing and engraftment of BCR-ABL11 leukemic stem cells in the bone marrow niche. Blood 12:1361–1372
41. Ley K, Laudanna C, Cybulsky MI, Nourshargh S (2007) Getting to the site of inflammation: the leukocyte adhesion cascade updated. Nat Rev Immunol 7:678–689
42. Chang P, Qu Y, Liu Y, Cui S, Zhu D, Wang H, Jin X (2013) Multitherapeutic effects of human adipose-derived mesenchymal stem cells on radiation-induced intestinal injury. Cell Death Dis 13: 685–696
43. Klopp AH, Spaeth EL, Dembinski JL, Woodward WA, Munshi A, Meyn RE, Cox JD, Andreeff M, Marini FC (2007) Tumor irradiation increases the recruitment of circulating mesenchymal stem cells into the tumor microenvironment. Cancer Res 67:11687–11695
44. Ziadloo A, Burks SR, Gold EM, Lewis BK, Chaudhry A, Merino MJ, Frenkel V, Frank JA (2012) Enhanced homing permeability and retention of bone marrow stromal cells by noninvasive pulsed focused ultrasound. Stem Cells 30(6):1216–1227
45. Burks SR, Ziadloo A, Kim SJ, Nguyen BA, Frank JA (2013) Noninvasive pulsed focused ultrasound allows spatiotemporal control of targeted homing for multiple stem cell types in murine skeletal muscle and the magnitude of cell homing can be increased through repeated applications. Stem Cells 31:2551–2560
46. Tempany CM, McDannold NJ, Hynynen K, Jolesz FA (2011) Focused ultrasound surgery in oncology: overview and principles. Radiology 259:39–56
47. Orsi F, Zhang L, Arnone P, Orgera G, Bonomo G, Vigna PD, Monfardini L, Zhou K, Chen W, Wang Z, Veronesi U (2010) High-intensity focused ultrasound ablation: effective and safe therapy for solid tumors in difficult locations. AJR Am J Roentgenol 195:245–252